

How to cite: *Angew. Chem. Int. Ed.* **2023**, *62*, e202215057

International Edition: doi.org/10.1002/anie.202215057

German Edition: doi.org/10.1002/ange.202215057

Atomically Dispersed Nickel Anchored on a Nitrogen-Doped Carbon/TiO₂ Composite for Efficient and Selective Photocatalytic CH₄ Oxidation to Oxygenates

Hui Song⁺, Hengming Huang⁺, Xianguang Meng,^{*} Qi Wang, Huilin Hu, Shengyao Wang, Hongwei Zhang, Wipakorn Jewasawan, Naoki Fukata, Ningdong Feng,^{*} and Jinhua Ye^{*}

Abstract: Direct photocatalytic oxidation of methane to liquid oxygenated products is a sustainable strategy for methane valorization at room temperature. However, in this reaction, noble metals are generally needed to function as cocatalysts for obtaining adequate activity and selectivity. Here, we report atomically dispersed nickel anchored on a nitrogen-doped carbon/TiO₂ composite (Ni–NC/TiO₂) as a highly active and selective catalyst for photooxidation of CH₄ to C1 oxygenates with O₂ as the only oxidant. Ni–NC/TiO₂ exhibits a yield of C1 oxygenates of 198 μmol for 4 h with a selectivity of 93%, exceeding that of most reported high-performance photocatalysts. Experimental and theoretical investigations suggest that the single-atom Ni–NC sites not only enhance the transfer of photogenerated electrons from TiO₂ to isolated Ni atoms but also dominantly facilitate the activation of O₂ to form the key intermediate •OOH radicals, which synergistically lead to a substantial enhancement in both activity and selectivity.

Introduction

Methane is not only a highly available clean fuel from natural gas, shale gas and biogas, but also a very potent and important greenhouse gas with a warming potential more than 25 times that of CO₂.^[1–3] The catalytic conversion of methane to higher added-value chemicals, typically derived from petroleum and coal, is therefore attractive for reducing dependence on crude oil and mitigating global warming. The current industrial methane conversion technology is

realized through an indirect route, associated with an energy-intensive syngas production process and the subsequent methanol or Fisher-Tropsch synthesis.^[3,4] Direct conversion of methane to methanol and other oxygenates with molecular oxygen is one of the most ideal approaches to realize methane transformation more efficiently and cleanly.^[5–9] The key challenge in direct methane conversion is the activation and selective oxidation of methane, because methane is a rather inert molecule and the desired products are more reactive than methane and is susceptible to

[*] H. Song,⁺ H. Huang,⁺ Q. Wang, W. Jewasawan, N. Fukata, J. Ye
International Center for Materials Nanoarchitectonics (WPI-MANA), National Institute for Materials Science (NIMS)
1-1 Namiki, Tsukuba, Ibaraki 305-0044 (Japan)
E-mail: Jinhua.YE@nims.go.jp

H. Huang⁺
State Key Laboratory of Materials-Oriented Chemical Engineering,
College of Materials Science and Engineering, Nanjing Tech
University
Nanjing 210009 (P. R. China)

X. Meng
Hebei Provincial Laboratory of Inorganic Nonmetallic Materials,
College of Materials Science and Engineering, North China
University of Science and Technology
Tangshan 063210 (P. R. China)
E-mail: mengxg_materchem@163.com

Q. Wang, J. Ye
Graduate School of Chemical Sciences and Engineering, Hokkaido
University
Sapporo 060-0814 (Japan)

H. Hu, J. Ye
TJU-NIMS International Collaboration Laboratory, School of Material Science and Engineering, Tianjin University
Tianjin 300072 (P. R. China)

S. Wang
College of Science, Huazhong Agricultural University
Wuhan 430070 (P. R. China)

H. Zhang
Biogas Institute of Ministry of Agriculture and Rural Affairs
Chengdu 610041 (P. R. China)

N. Feng
State Key Laboratory of Magnetic Resonance and Atomic and
Molecular Physics, National Center for Magnetic Resonance in
Wuhan, CAS Key Laboratory of Magnetic Resonance in Biological
Systems, Wuhan Institute of Physics and Mathematics, Innovation
Academy for Precision Measurement Science and Technology,
Chinese Academy of Sciences
Wuhan (P. R. China)
E-mail: ningdong.feng@wipm.ac.cn

[+] These authors contributed equally to this work.

© 2022 The Authors. *Angewandte Chemie International Edition* published by Wiley-VCH GmbH. This is an open access article under the terms of the Creative Commons Attribution License, which permits use, distribution and reproduction in any medium, provided the original work is properly cited.

overoxidation to CO_2 .^[6,7] To minimize the overoxidation of oxygenates, the methane conversion reaction is generally conducted at relatively low temperatures ($<200^\circ\text{C}$), along with the utilization of corrosive or expensive oxidants (such as sulfuric acid, N_2O , H_2O_2) to replace O_2 to activate methane and/or the operation of a stepwise chemical looping process, which makes the process economically uncompetitive.^[5-7,10,11]

Compared with thermocatalytic methane conversion, photocatalytic methane oxidation can proceed at room temperature to achieve appreciable yields of oxygenates and has recently received great interest.^[12-23] Cocatalysts play a vital role in semiconductor-based photocatalytic methane oxidation reactions, as they can not only promote the separation and transfer of photogenerated charge carriers, but also control the activation of reactants, thereby enhancing surface reaction rates and tuning product selectivity. Among various cocatalysts, noble metals generally exhibit the outstanding performance for photocatalytic methane oxidation.^[15,16,19,20,22-25] For example, our previous studies showed that noble metals (Pt, Pd, Au or Ag) decorated ZnO were active and selective for photooxidation of CH_4 with O_2 to oxygenates (CH_3OOH , CH_3OH and HCHO) and $\text{Ag}/\text{TiO}_2[001]$ enabled the selective production of CH_3OH , while pristine ZnO and TiO_2 exhibited low activity and selectivity for the production of oxygenates.^[20,23] Other researchers have also reported a series of good photocatalysts with noble metals as cocatalyst for photocatalytic aerobic oxidation of methane to oxygenates, such as $\text{Au-Pd}/\text{TiO}_2$,^[26] $\text{Pd}/\text{In}_2\text{O}_3$,^[16] Au/WO_3 ,^[25] Pt/WO_3 ^[24] and black phosphorous-supported Au single atoms.^[19]

Despite the promising results obtained in the above-mentioned studies, the high-cost and limited-reserves of noble metals limits their applications. Therefore, there is a high demand to develop low-cost and high-performance alternative cocatalysts to noble metals. Atomically dispersed non-precious metal atoms anchored on N-doped carbon (M-NC) materials, which are generally considered as single atomic site catalysts, have been employed as cocatalysts for efficient photocatalytic reactions such as H_2 production and CO_2 reduction,^[27-29] due to the highly exposed active metal sites and efficient transfer of charge carriers. Moreover, the electronic structure of atomic metal sites can be fine-tuned by changing the coordination environments, rendering M-NC active and selective for targeted catalytic reactions with favorable reaction kinetics.^[27,30] In view of such distinctive characteristics, M-NC potentially have the capability to enhance the activity and selectivity of semiconductor-based photocatalysts in photooxidation of CH_4 . Nevertheless, to the best of our knowledge, there have been no studies reporting the utilization of M-NC as cocatalysts for photocatalytic CH_4 oxidation.

In this work, a single-atom Ni-NC/ TiO_2 composite is prepared and used as a photocatalyst for direct CH_4 oxidation with O_2 to produce liquid oxygenates. We found that owing to the unique structural properties, the atomically dispersed Ni-NC sites not only promote the carrier separation and transfer efficiency, but also enable the controlled activation of O_2 to $\cdot\text{OOH}$ radicals, a key intermediate for

the formation of the primary product CH_3OOH that can be readily transformed into CH_3OH and HCHO . As a result, a high C1 oxygenates yield of up to $198 \mu\text{mol}$ with 93% selectivity is achieved after 4 h of irradiation, superior to most previously reported photocatalysts using noble metals as cocatalysts.

Results and Discussion

Figure 1a illustrates the synthetic process for the preparation of Ni-NC/ TiO_2 via a facile one-pot solvothermal method.^[31] Briefly, TiO_2 (P25) and Ni precursor (NiCl_2) were first dispersed in formamide (HCONH_2). Then, the mixed solution was solvothermally heated at 180°C for 12 h. During the solvothermal process, formamide can be easily transformed into nitride-doped carbon (NC) material on the surface of TiO_2 ; meanwhile, considering the strong interaction of Ni-N coordination, Ni-N bond was formed in the presence of Ni^{2+} . Finally, the resulting sample was washed with diluted acid and water for several times to yield TiO_2 loaded with NC coordinated Ni catalyst (denoted as Ni-NC/ TiO_2). The color of the material after solvothermal reaction changed from white to black (Figure S1), indicative of loading of Ni and CN on TiO_2 . The Fourier-transform infrared (FT-IR) spectra show a new peak at 1386 cm^{-1} on Ni-NC/ TiO_2 (Figure S2), confirming the presence of C-N groups. Inductively coupled plasma optical emission spectrometry shows that the weight amount of Ni in Ni-NC/ TiO_2 is 0.5 wt %. For comparison, TiO_2 decorated with Ni nanoparticles (NPs) with a loading amount of 0.5 wt % (denoted as Ni NPs/ TiO_2) was prepared via an impregnation method followed by H_2 reduction at 400°C for 1 h.

X-ray diffraction (XRD) patterns (Figure 1b) show that all diffraction peaks are associated with TiO_2 (anatase and rutile) and no peak of any likely Ni species is observed on Ni-NC/ TiO_2 and Ni NPs/ TiO_2 .^[32] Transmission electron microscopy (TEM) and high-resolution TEM images (Figure 1c-e) show that the surface of TiO_2 is wrapped by a thin amorphous layer in Ni-NC/ TiO_2 and no sign of remarkable Ni NPs is detected, while small Ni NPs with size of 2–3 nm were formed on TiO_2 surface in Ni NPs/ TiO_2 (Figure S3). Two lattice fringes with interplanar distances of 0.352 and 0.325 nm agree well with the crystal parameters of anatase (101) and rutile (110) planes, respectively, implying that solvothermal treatment did not alter the crystal structure of TiO_2 (Figure 1d and e). Aberration-corrected high-angle annular dark-field scanning TEM (AC HAADF-STEM) image shows many isolated bright spots with no observed clusters or subnanoparticles in Ni-NC/ TiO_2 (Figure 1f), which directly validates the formation of atomically dispersed Ni sites. The energy dispersive X-ray (EDX) spectroscopy elemental mapping analysis (Figure 1g) demonstrates that elemental Ni is uniformly dispersed throughout the entire structure of Ni-NC/ TiO_2 .

The surface compositions and chemical states of Ni-NC/ TiO_2 were investigated by X-ray photoelectron spectroscopy (XPS). The high-resolution Ni 2p XPS spectrum of Ni-NC/ TiO_2 (Figure 2a) displays the binding energy of Ni 2p_{3/2} peak

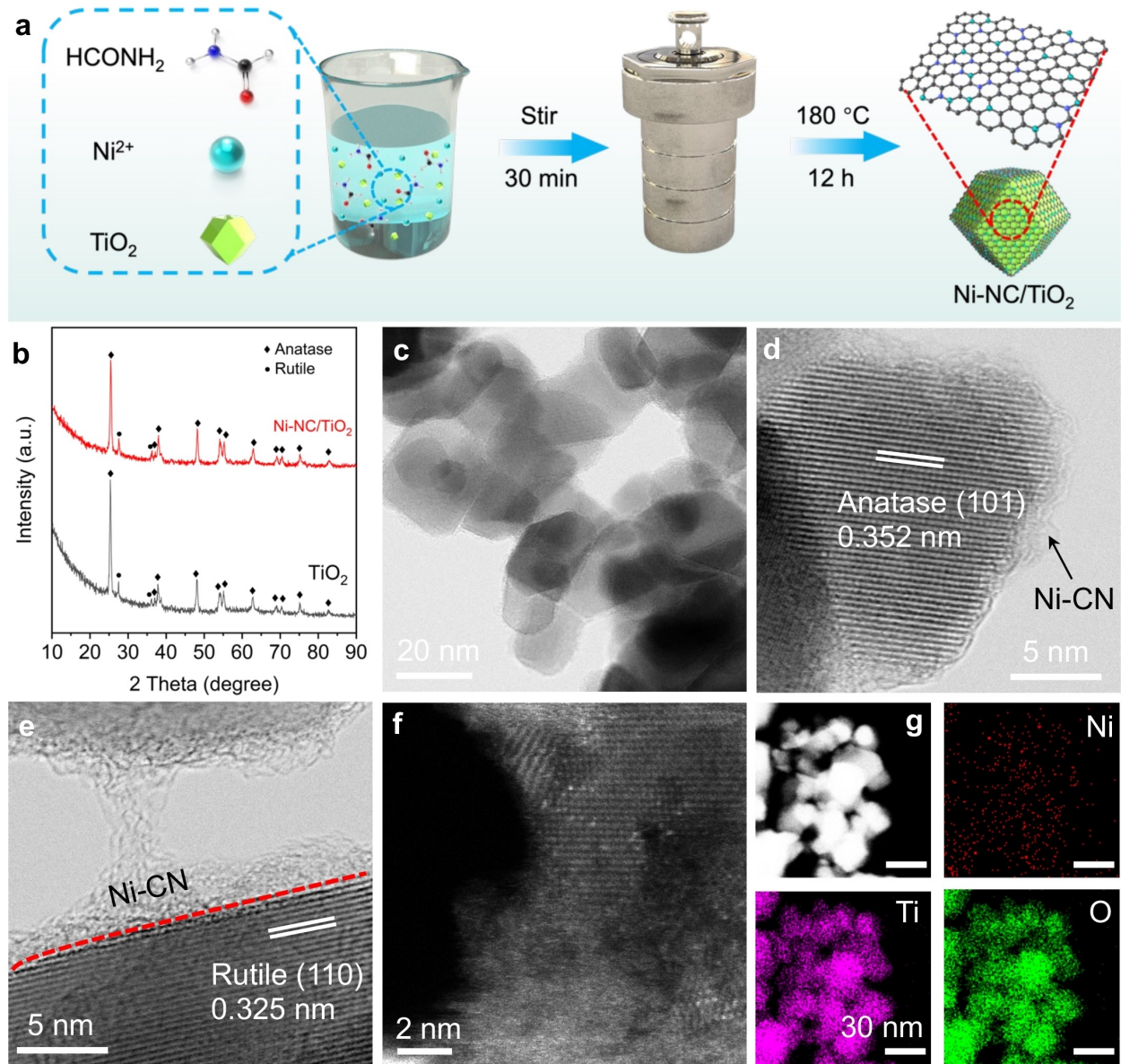


Figure 1. Schematic illustration and morphology characterizations of Ni-NC/TiO₂. a) Schematic illustration of the synthetic procedure of Ni-NC/TiO₂. b) XRD patterns of Ni-NC/TiO₂ and TiO₂. c) TEM image of Ni-NC/TiO₂. d) and e) HR-TEM images of Ni-NC/TiO₂. f) AC HADDF-STEM image of Ni-NC/TiO₂. g) EDX elemental mapping images of Ni-NC/TiO₂.

at 855.2 eV, which is higher than that of Ni⁰ (853.5 eV) and slightly lower than that of Ni²⁺ (855.8 eV),^[33,34] suggesting the formation of positively charged Ni species. The high-resolution N 1s spectrum of Ni-NC/TiO₂ is deconvoluted into three characteristic peaks at 398.8 eV, 399.7 eV and 400.7 eV (Figure S4), which could be assigned to pyridinic-N, Ni-N and pyrrolic-N,^[35] respectively. The presence of Ni-N species indicates that Ni atoms are adequately coordinated with N sites.

X-ray absorption fine structure spectroscopy (XAFS) analysis was further performed to investigate the coordination environment of Ni in Ni-NC/TiO₂ using Ni foil, NiO and nickel phthalocyanine (NiPc) as references. The Ni K-edge X-ray absorption near-edge structure (XANES) spec-

tra (Figure 2b) show that the absorption edge position of Ni-NC/TiO₂ is between those of Ni foil and NiO, revealing the cationic Ni sites, in good consistency with the result of XPS analysis. Additionally, Ni-NC/TiO₂ has a similar pre-edge profile to NiPc with a peak at 8340 eV, which is attributed to the transition of 1s to 4p and is the feature of planar Ni-N₄ moiety.^[33] Compared with NiPc, the slight decrease in light intensity of Ni-NC/TiO₂ probably results from the distorted Ni-N₄ structure. As shown in the Fourier transformed (FT) Ni K-edge extended XAFS (EXAFS) spectra (Figure 2c), the prominent peak at ca.1.40 Å for Ni-NC/TiO₂ corresponds to first shell coordination of Ni-N bond,^[36] contributing similarly to the NiPc reference, and no obvious Ni-Ni peak at 2.19 Å is detected, revealing the

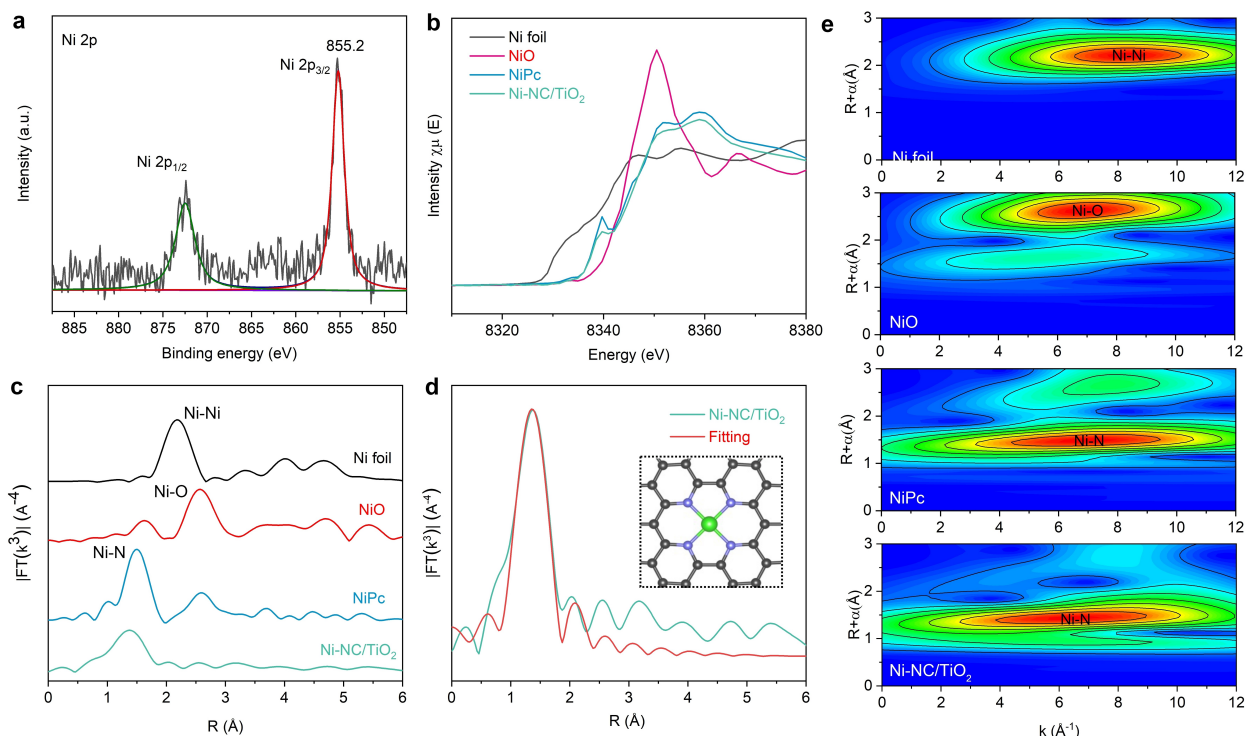


Figure 2. Structural characterizations of Ni–NC/TiO₂. a) Ni 2p XPS spectrum of Ni–NC/TiO₂. b) Ni K-edge XANES spectra. c) FT Ni K-edge EXAFS spectra of Ni–NC/TiO₂, Ni foil, NiO and NiPc. The prominent peak of Ni–NC/TiO₂ is similar to that of NiPc, confirming the presence of Ni–N coordination. d) EXAFS fitting curve of Ni–NC/TiO₂. The inset is the model Ni–N₄ structure. Ni, green; N, blue; C, black. The Ni site in Ni–NC/TiO₂ matches well with a Ni–N₄ site configuration. e) WT-EXAFS spectra of Ni foil, NiO, NiPc and Ni–NC/TiO₂.

negligible presence of metallic Ni species. These results confirm the presence of atomic dispersion of Ni species in Ni–NC/TiO₂ in the form of Ni–N coordination, in accordance with the result of dispersed Ni atoms from HAADF-STEM image. To precisely quantify the coordination micro-environment of Ni site, the curve fitting for EXAFS spectra was performed (Figure 2d, Figure S5, and Table S1). As shown in Figure 2d, the fitting results of the first coordination shell verify that the Ni site in Ni–NC/TiO₂ is four-coordinated by N atoms, matching well with a Ni–N₄ site configuration. In addition, the wavelet transform EXAFS (WT-EXAFS) spectra (Figure 2e) show that Ni–NC/TiO₂ and NiPc exhibit similar contour plot with only one intensity maximum at 6.5 Å⁻¹ instead of the Ni–Ni interaction (c.a. 8.4 Å⁻¹).^[37] This further manifests the formation of dispersed Ni atoms with Ni–N coordination. All of above characterizations demonstrate that Ni species are atomically dispersed in Ni–NC/TiO₂ with Ni–N₄ moiety.

Photocatalytic CH₄ oxidation performance was evaluated in a batch reactor at room temperature using only O₂ as the oxidant.^[22,23] As shown in Figure 3a, only HCHO was detected in the liquid phase over pristine TiO₂ after 4 h of irradiation with a yield of 140 μmol, accompanied by 33 μmol of CO₂. For Ni NPs/TiO₂, the yields of HCHO and CO₂ slightly decreased to 135 and 26 μmol, respectively, with the production of a small amount of CH₃OH (19 μmol). The selectivity for C1 oxygenated products increased from ≈81 % over pristine TiO₂ to ≈86 % over Ni NPs/TiO₂. Due

to CH₃OH being the precursor of HCHO and CO₂ in the photocatalytic CH₄ oxidation,^[22,23] the trace or small amount of CH₃OH observed over TiO₂ and Ni NPs/TiO₂ suggests the facile overoxidation of CH₄. By comparison, a much higher yield of primary products CH₃OOH (55 μmol) and CH₃OH (29 μmol) together with 114 μmol of HCHO were produced over Ni–NC/TiO₂, and the amount of CO₂ decreased to 16 μmol. This leads to a remarkable ≈93 % oxygenates selectivity and the corresponding apparent quantum efficiency (AQE) for oxygenates at 360 nm was determined to be 1.9 %. The yield and selectivity of liquid oxygenates of Ni–NC/TiO₂ are higher than those of Ni–NPs/TiO₂ and TiO₂, demonstrating the superiority of single atom Ni–NC cocatalysts for the photocatalytic CH₄ oxidation. The excellent photocatalytic performance observed over Ni–NC/TiO₂ is comparable to or even outperforms most reported photocatalysts decorated with either noble metal or non-noble metal cocatalysts under similar experiment conditions (Table S2).^[12,13,16,17,19,20,22–25,38–40]

Reactions without photocatalyst, without light or replacing CH₄ with Ar did not yield any product. Isotope labelling experiment using ¹³CH₄ was performed to elucidate the source of carbon atoms of the products. ¹³C NMR spectrum shows three obvious peaks assigned to CH₃OOH, CH₃OH and HCHO (Figure 3b), suggesting that the produced oxygenates originated from methane, instead of carbon materials in Ni–NC/TiO₂. In addition, no liquid products were detected without the introduction of O₂ (Figure S6), which

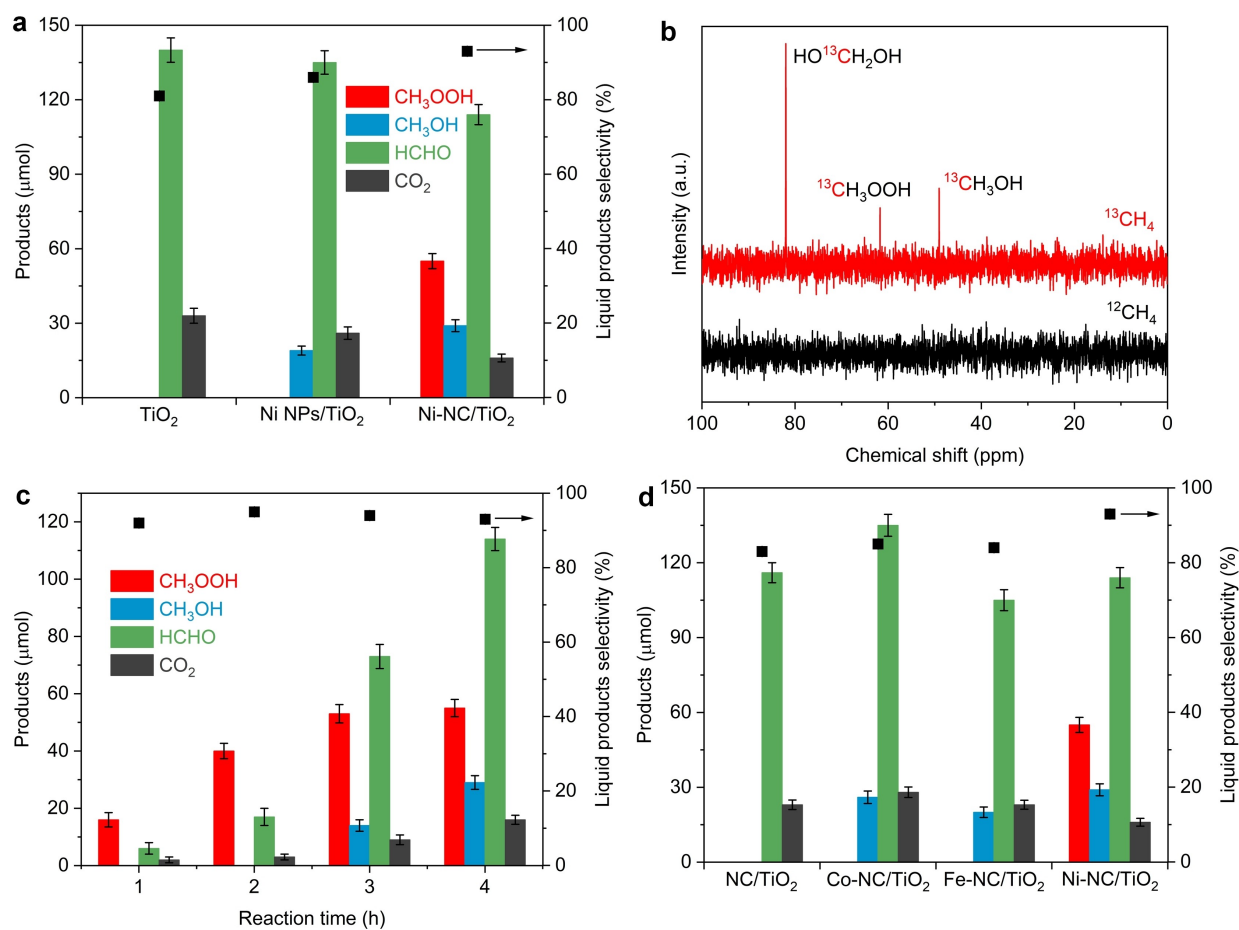


Figure 3. The photocatalytic performance of CH_4 oxidation with O_2 . a) Yields of oxygenated products and the selectivity of liquid products over TiO_2 , Ni-NC/TiO_2 , and Ni NPs/TiO_2 after 4 h of light irradiation. b) ^{13}C NMR spectrum of liquid products over Ni-NC/TiO_2 using 0.8 MPa $^{13}\text{CH}_4$ after 6 h of light irradiation. c) Yields of oxygenated products and the selectivity of liquid products over Ni-NC/TiO_2 under different irradiation time. d) Yields of oxygenated products and the selectivity of liquid products over different photocatalysts after 4 h of light irradiation. Error bars represent standard deviations of three replicate measurements.

indicates that O_2 is the necessary for photocatalytic CH_4 oxidation. Isotopic experiments with oxygen revealed that O_2 molecules was the oxygen source of the produced oxygenates (Figure S7). The overall yield of oxygenates was increased with the reaction time, and the formation of CH_3OH was observed by extending the irradiation time over 3 h (Figure 3c). Increasing the water amount was conducive to promoting the production of oxygenates and suppressing the overoxidation of CH_4 to CO_2 (Figure S8). There was marginal loss in the photocatalytic performance and selectivity for oxygenates after consecutive five runs (Figure S9), and the morphology and structure of catalyst remained unchanged (Figures S10 and S11). These results confirm the good stability of Ni-NC/TiO_2 . Increasing the amount of Ni from 0.5 wt % to 1.1 wt % did not noticeably improve the performance of Ni-NC/TiO_2 (Figure S12), because excessive loading amount of Ni-CN can shield light absorption of TiO_2 (Figure S13). When Ni was replaced with Co and Fe, the total amounts of oxygenates were reduced, due to no detectable formation of CH_3OOH (Figure 3d). This demonstrates that the isolated Ni site in Ni-NC with

unique properties play an important role for efficient photo-oxidation of methane to oxygenates.

To understand the role of cocatalysts in photocatalytic reaction, the photoluminescence (PL) spectra of the samples were performed to study the photogenerated charge separation efficiency (Figure 4a). Bare TiO_2 shows an intensive emission peak at 400–440 nm upon excitation at 320 nm. After the introduction of Ni NPs or Ni-NC on TiO_2 , the PL intensity is remarkably decreased, and Ni-NC/TiO_2 exhibits a lower emission peak than Ni NP/TiO_2 , indicating that Ni-NC favorably prevents the recombination of charge carriers compared to Ni NPs cocatalysts. The time-resolved PL spectra were carried out to investigate the dynamics of charge carriers (Figure 4b). The average lifetime of Ni-NC/TiO_2 (0.9 ns) is shorter than those of Ni NP/TiO_2 (1.9 ns) and TiO_2 (4.5 ns), in line with the typical cocatalyst/semiconductor systems in which the facile electrons transfer from semiconductors to cocatalysts leads to fast fluorescence decay,^[41,42] revealing the excellent ability of Ni-NC to accelerate the transfer of photogenerated electrons. These results demonstrate the positive role of Ni-NC in efficiently

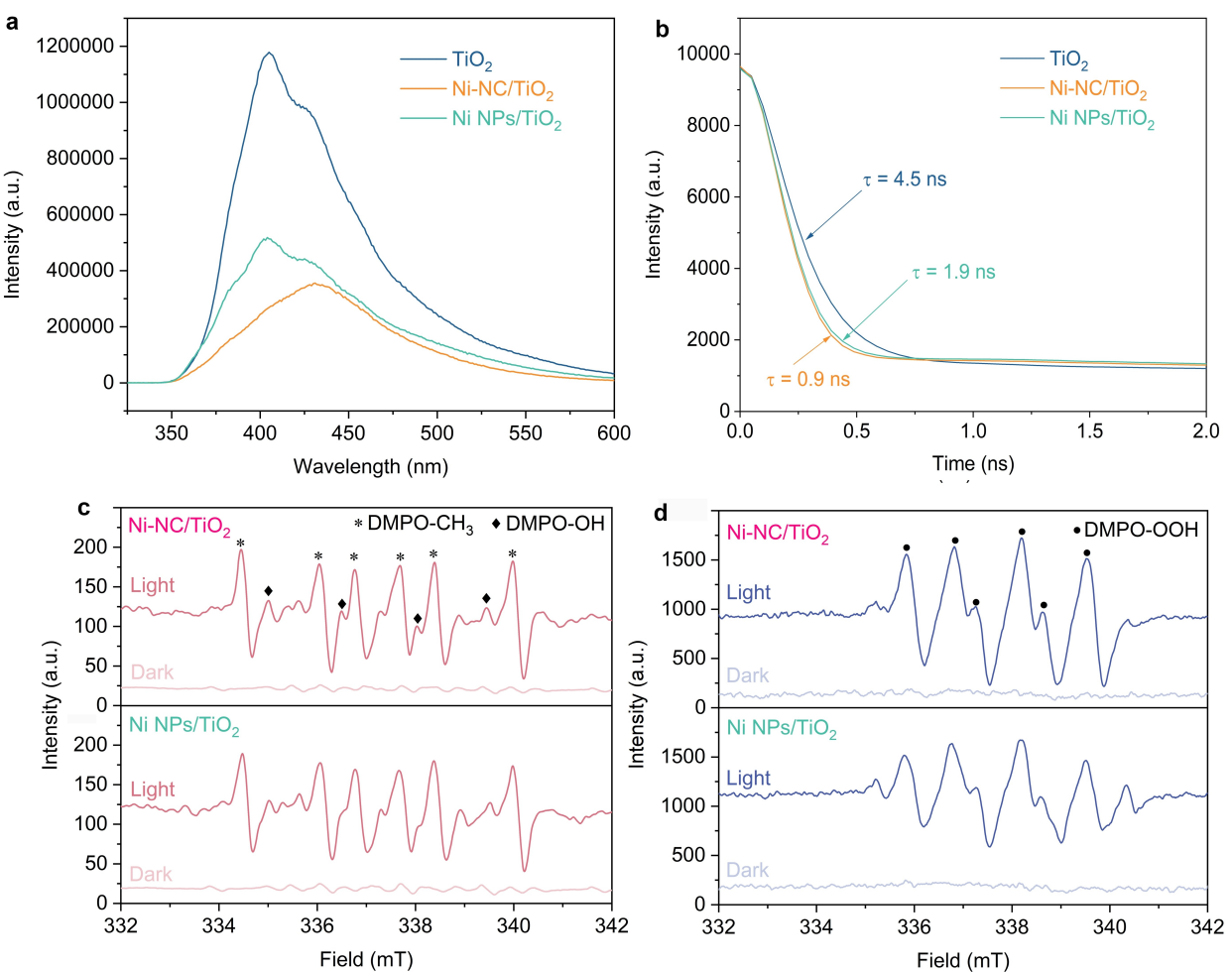


Figure 4. Mechanistic investigation of photocatalytic CH₄ oxidation. a) PL spectra and b) Time-resolved PL decay plots of TiO₂, Ni–NC/TiO₂, and Ni NPs/TiO₂. EPR spectra for detecting •CH₃ radicals (c) and •OOH radicals (d) over Ni–NC/TiO₂ and Ni NPs/TiO₂ under dark and light irradiation.

separating electrons and holes, thereby leading to the enhanced performance of photocatalytic CH₄ oxidation.

Generally, for photocatalytic CH₄ aerobic reaction in aqueous solution, the C–H bond of CH₄ is oxidized by photo-generated active oxygen species to form •CH₃ radicals, which would react with oxygen-derived free radicals to produce oxygenates.^[23] To elucidate the reaction mechanism of photocatalytic CH₄ oxidation, electron paramagnetic resonance (EPR) with 5,5-dimethyl-1-pyrroline-N-oxide (DMPO) was conducted. As shown in Figure 4c, •CH₃ radicals are detected on both Ni–NC/TiO₂ and Ni NP/TiO₂, and the intensities of •CH₃ radicals of Ni–NC/TiO₂ is slightly higher than that of Ni NP/TiO₂, revealing that the activation of CH₄ to •CH₃ radicals occurs in selective photo-oxidation of CH₄ in aqueous solution. Figure S14 shows that strong EPR signals assigned to •OH radicals are observed without the introduction of CH₄. The decreased intensity of •OH radicals in the presence of CH₄ may be due to the highly active •OH radicals participating in CH₄ oxidation, such as deep oxidation of CH₄ to HCHO and CO₂.^[22] For the intermediates in photocatalytic O₂ reduction, one set of EPR signals that are assigned to •OOH radicals appear

upon illumination (Figure 4d). The observed •OOH radicals are easily produced from O₂ reduction with protons by photogenerated electrons. Clearly, the signal intensity of •OOH radicals of Ni–NC/TiO₂ is higher than that of Ni NP/TiO₂, indicating that Ni–CN cocatalyst can facilitate the formation of •OOH radicals compared with Ni NP cocatalyst. The high amount of •OOH radicals probably lead to the enhanced production of CH₃OOH and other oxygenates.

Based on the above results, a plausible photocatalytic CH₄ oxidation mechanism on Ni–NC/TiO₂ is depicted in Figure S15. Under light irradiation, electrons and holes are generated on TiO₂. The photogenerated electrons are transferred to single Ni–NC sites to promote the reduction of O₂ to form •OOH radicals, while the powerful holes are left on the surface of TiO₂ to initiate the CH₄ oxidation to produce •CH₃ radicals. These two radicals can easily combine to form the primary product CH₃OOH, which can be subsequently transformed into CH₃OH and HCHO. The single Ni–NC sites guarantee the efficient separation of photogenerated electrons and holes and the favourable formation of •OOH radicals by mild reduction of O₂, ultimately leading to excellent performance of photocata-

lytic CH_4 oxidation with O_2 . To demonstrate this hypothesis, the detailed reaction pathways were calculated by density functional theory (DFT) calculations. The optimized structural models of Ni–NC/TiO₂ and Ni NPs/TiO₂ are given in Figure S16.

The energy profiles of the O_2 reduction and CH_4 activation reactions are illustrated in Figure 5a and b, with the corresponding structures of reaction intermediates and transition states shown in Figure 5c and d. The activation of O_2 to form *OOH species is an exothermic reaction on Ni–NC/TiO₂ and Ni NPs/TiO₂, with a reaction energy of -0.79 and -2.85 eV, respectively. The comparatively unfavorable formation of *OOH species indicates the weak surface adsorption of Ni–NC because of its unique electronic structure. This results in the preferential desorption of *OOH species to generate •OH radicals that can participate in the production of CH_3OOH , instead of the subsequent dissociation of *OOH to form •OH radicals due to the large reaction energy (2.00 eV). By contrast, the

desorption energy of *OOH species on Ni NPs is as high as 2.62 eV. Compared with *OOH desorption, the dissociation of *OOH to *O + *OH is more preferred on Ni NPs, with a reaction energy of -2.25 eV and an energy barrier of 0.12 eV, and the produced *OH species on Ni NPs could desorb to form •OH radicals for oxidizing oxygenates to CO_2 . These results indicate that Ni–NC cocatalyst is beneficial for the production of •OOH radicals in O_2 reduction, consistent with the EPR results, which contributes to the production of oxygenates. The different behaviors of Ni NPs and Ni–NC on O_2 activation probably because *OOH is very unstable on metallic Ni NPs and is easily dissociated to form strong Ni–O bonds, as indicated by the large reaction energy (-2.25 eV), while Ni–NC is stabilized by N coordination, thus unfavorable for further dissociation of *OOH.

For CH_4 activation, the reaction energy for the cleavage of the first C–H bond of 1.14 eV on Ni–NC/TiO₂ is quite similar to that on Ni NPs/TiO₂ (1.15 eV), with a relatively

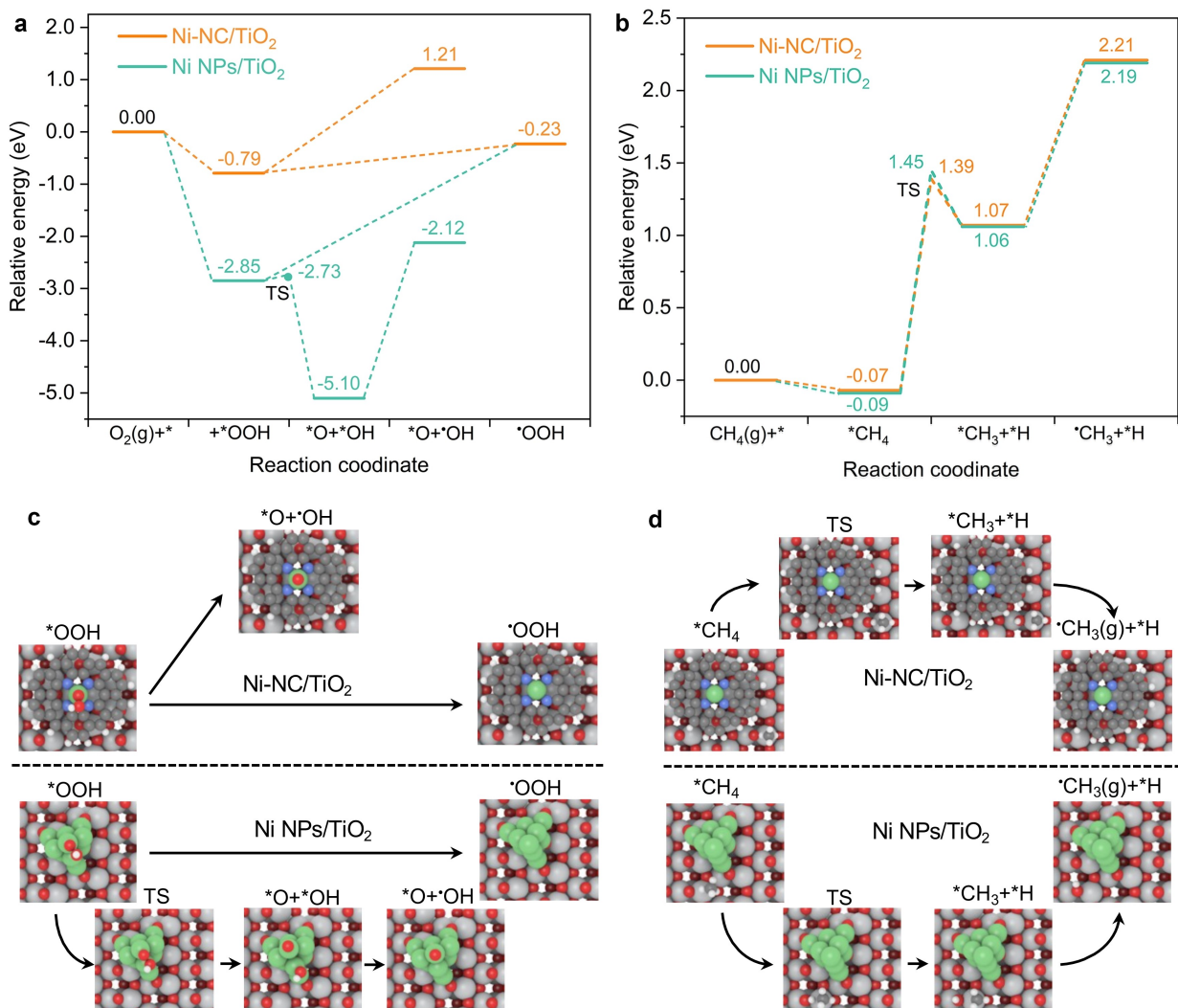


Figure 5. Calculated reaction energy of O_2 and CH_4 activation on Ni–NC/TiO₂ and Ni NPs/TiO₂. a) Energy profiles of O_2 reduction to *OOH and •OH radicals. b) Energy profiles of CH_4 activation to *CH₃ radicals. c) and d) The structures of reaction intermediates and transition states (TS). Ni, green; N, blue; C, black; O, red; Ti, gray.

lower energy barrier (1.46 eV vs. 1.54 eV). Likewise, the reaction energies for the subsequent $^*\text{CH}_3$ desorption to $^*\text{CH}_3$ radicals on Ni–NC/TiO₂ and Ni NPs/TiO₂ are similar (1.14 eV vs. 1.13 eV). It clearly shows that there is no significant difference in the activation of methane over Ni–NC and Ni NPs cocatalysts. As a result, the different pathways of O₂ reduction over Ni–NC/TiO₂ and Ni NP/TiO₂ primarily contribute to the differences of activity and selectivity in photocatalytic CH₄ oxidation.

Conclusion

In summary, atomically dispersed Ni–NC/TiO₂ has been developed by a facile one-pot solvothermal method for room-temperature photocatalytic CH₄ oxidation with O₂ to C1 oxygenates with 93 % selectivity. The single-atom Ni–NC sites function as electron capture centers to achieve efficient separation of charge carriers in Ni–NC/TiO₂. Moreover, the isolated Ni atoms are active for the favorable formation and desorption of $^*\text{OOH}$ radicals in O₂ reduction, rather than being active for the production of $^*\text{OH}$ radicals that are more likely to facilitate the overoxidation of oxygenates to CO₂. Such unique properties of Ni–NC results in a prominent C1 oxygenates productive rate and high selectivity. This work is the first case of single metal atoms anchored N-doped carbon material as a cocatalyst to promote the performance of photocatalytic aerobic oxidation of CH₄, which may drive the discovery of more earth-abundant and low-cost photocatalysts for efficiently and selectively oxidizing CH₄ to solar fuels and chemicals.

Acknowledgements

This work received partial financial support from JSPS KAKENHI Grant Number JP18H02065, Photo-excitonix Project in Hokkaido University, National Natural Science Foundation of China (Nos. 51872091, 22127801 and 22002060), State Scholarship Fund by China Scholarship Council (CSC) (No. 202008320109), and Priority Academic Program Development of the Jiangsu Higher Education Institutions (PAPD).

Conflict of Interest

The authors declare no conflict of interest.

Data Availability Statement

The data that support the findings of this study are available from the corresponding author upon reasonable request.

Keywords: Oxygenates · Photocatalysis · Selective Methane Oxidation · Single Ni–NC Sites · TiO₂

- [1] L. Yuliati, H. Yoshida, *Chem. Soc. Rev.* **2008**, *37*, 1592.
- [2] X. Li, C. Wang, J. Tang, *Nat. Rev. Mater.* **2022**, *7*, 617.
- [3] H. Song, X. Meng, Z.-j. Wang, H. Liu, J. Ye, *Joule* **2019**, *3*, 1606.
- [4] X. Meng, X. Cui, N. P. Rajan, L. Yu, D. Deng, X. Bao, *Chem* **2019**, *5*, 2296.
- [5] S. J. Freakley, N. Dimitratos, D. J. Willock, S. H. Taylor, C. J. Kiely, G. J. Hutchings, *Acc. Chem. Res.* **2021**, *54*, 2614.
- [6] M. Ravi, V. L. Sushkevich, A. J. Knorpp, M. A. Newton, D. Palagin, A. B. Pinar, M. Ranocchiari, J. A. van Bokhoven, *Nat. Catal.* **2019**, *2*, 485.
- [7] M. Ravi, M. Ranocchiari, J. A. van Bokhoven, *Angew. Chem. Int. Ed.* **2017**, *56*, 16464; *Angew. Chem.* **2017**, *129*, 16684–16704.
- [8] S. Song, H. Song, L. Li, S. Wang, W. Chu, K. Peng, X. Meng, Q. Wang, B. Deng, Q. Liu, *Nat. Catal.* **2021**, *4*, 1032.
- [9] H. Song, J. Ye, *Trends Chem.* **2022**, *4*, 1094–1105.
- [10] Q. Li, Y. Ouyang, H. Li, L. Wang, J. Zeng, *Angew. Chem. Int. Ed.* **2022**, *61*, e202108069; *Angew. Chem.* **2022**, *134*, e202108069.
- [11] A. I. Olivos-Suarez, Á. Szécsényi, E. J. M. Hensen, J. Ruiz-Martinez, E. A. Pidko, J. Gascon, *ACS Catal.* **2016**, *6*, 2965.
- [12] K. Zheng, Y. Wu, J. Zhu, M. Wu, X. Jiao, L. Li, S. Wang, M. Fan, J. Hu, W. Yan, J. Zhu, Y. Sun, Y. Xie, *J. Am. Chem. Soc.* **2022**, *144*, 12357.
- [13] P. Xie, J. Ding, Z. Yao, T. Pu, P. Zhang, Z. Huang, C. Wang, J. Zhang, N. Zecher-Freeman, H. Zong, D. Yuan, S. Deng, R. Shahbazian-Yassar, C. Wang, *Nat. Commun.* **2022**, *13*, 1375.
- [14] Y. Wang, J. Zhang, W.-X. Shi, G.-L. Zhuang, Q.-P. Zhao, J. Ren, P. Zhang, H.-Q. Yin, T.-B. Lu, Z.-M. Zhang, *Adv. Mater.* **2022**, *34*, 2204448.
- [15] L. Luo, Z. Gong, Y. Xu, J. Ma, H. Liu, J. Xing, J. Tang, *J. Am. Chem. Soc.* **2022**, *144*, 740.
- [16] L. Luo, L. Fu, H. Liu, Y. Xu, J. Xing, C.-R. Chang, D.-Y. Yang, J. Tang, *Nat. Commun.* **2022**, *13*, 2930.
- [17] Y. Jiang, W. Zhao, S. Li, S. Wang, Y. Fan, F. Wang, X. Qiu, Y. Zhu, Y. Zhang, C. Long, Z. Tang, *J. Am. Chem. Soc.* **2022**, *144*, 15977.
- [18] B. An, Z. Li, Z. Wang, X. Zeng, X. Han, Y. Cheng, A. M. Sheveleva, Z. Zhang, F. Tuna, E. J. L. McInnes, M. D. Frogley, A. J. Ramirez-Cuesta, L. S. Natrajan, C. Wang, W. Lin, S. Yang, M. Schröder, *Nat. Mater.* **2022**, *21*, 932.
- [19] L. Luo, J. Luo, H. Li, F. Ren, Y. Zhang, A. Liu, W.-X. Li, J. Zeng, *Nat. Commun.* **2021**, *12*, 1218.
- [20] N. Feng, H. Lin, H. Song, L. Yang, D. Tang, F. Deng, J. Ye, *Nat. Commun.* **2021**, *12*, 4652.
- [21] Y. Fan, W. Zhou, X. Qiu, H. Li, Y. Jiang, Z. Sun, D. Han, L. Niu, Z. Tang, *Nat. Sustainability* **2021**, *4*, 509.
- [22] H. Song, X. Meng, S. Wang, W. Zhou, S. Song, T. Kako, J. Ye, *ACS Catal.* **2020**, *10*, 14318.
- [23] H. Song, X. Meng, S. Wang, W. Zhou, X. Wang, T. Kako, J. Ye, *J. Am. Chem. Soc.* **2019**, *141*, 20507.
- [24] Y. Zhu, S. Chen, S. Fang, Z. Li, C. Wang, Y. H. Hu, *J. Phys. Chem. Lett.* **2021**, *12*, 7459.
- [25] S. Wei, X. Zhu, P. Zhang, Y. Fan, Z. Sun, X. Zhao, D. Han, L. Niu, *Appl. Catal. B* **2021**, *283*, 119661.
- [26] X. Cai, S. Fang, Y. H. Hu, *J. Mater. Chem. A* **2021**, *9*, 10796.
- [27] S. Ji, Y. Chen, X. Wang, Z. Zhang, D. Wang, Y. Li, *Chem. Rev.* **2020**, *120*, 11900.
- [28] Y. Li, S. Wang, P. Wang, Y. He, X. Wang, K. Chang, H. Lin, X. Ding, H. Chen, H. Zhang, *Nano Energy* **2020**, *76*, 105077.
- [29] G. Zhao, Y. Sun, W. Zhou, X. Wang, K. Chang, G. Liu, H. Liu, T. Kako, J. Ye, *Adv. Mater.* **2017**, *29*, 1703258.
- [30] J. Yang, Z. Sun, K. Yan, H. Dong, H. Dong, J. Cui, X. Gong, S. Han, L. Huang, J. Wen, *Green Chem.* **2021**, *23*, 2756.

- [31] X. Cui, H. Li, Y. Wang, Y. Hu, L. Hua, H. Li, X. Han, Q. Liu, F. Yang, L. He, X. Chen, Q. Li, J. Xiao, D. Deng, X. Bao, *Chem.* **2018**, *4*, 1902.
- [32] H. Song, X. Meng, Z.-j. Wang, Z. Wang, H. Chen, Y. Weng, F. Ichihara, M. Oshikiri, T. Kako, J. Ye, *ACS Catal.* **2018**, *8*, 7556.
- [33] H. B. Yang, S.-F. Hung, S. Liu, K. Yuan, S. Miao, L. Zhang, X. Huang, H.-Y. Wang, W. Cai, R. Chen, *Nat. Energy* **2018**, *3*, 140.
- [34] B. Seemala, C. M. Cai, C. E. Wyman, P. Christopher, *ACS Catal.* **2017**, *7*, 4070.
- [35] Y. Zhang, L. Jiao, W. Yang, C. Xie, H.-L. Jiang, *Angew. Chem. Int. Ed.* **2021**, *60*, 7607; *Angew. Chem.* **2021**, *133*, 7685.
- [36] Q. Fan, P. Hou, C. Choi, T.-S. Wu, S. Hong, F. Li, Y.-L. Soo, P. Kang, Y. Jung, Z. Sun, *Adv. Energy Mater.* **2020**, *10*, 1903068.
- [37] J. Yang, Z. Qiu, C. Zhao, W. Wei, W. Chen, Z. Li, Y. Qu, J. Dong, J. Luo, Z. Li, Y. Wu, *Angew. Chem. Int. Ed.* **2018**, *57*, 14095; *Angew. Chem.* **2018**, *130*, 14291.
- [38] P.-P. Luo, X.-K. Zhou, Y. Li, T.-B. Lu, *ACS Appl. Mater. Interfaces* **2022**, *14*, 21069.
- [39] M. Huang, S. Zhang, B. Wu, Y. Wei, X. Yu, Y. Gan, T. Lin, F. Yu, F. Sun, Z. Jiang, L. Zhong, *ACS Catal.* **2022**, *12*, 9515.
- [40] Z. Sun, C. Wang, Y. H. Hu, *J. Mater. Chem. A* **2021**, *9*, 1713.
- [41] L. Huang, J. Yang, X. Wang, J. Han, H. Han, C. Li, *Phys. Chem. Chem. Phys.* **2013**, *15*, 553.
- [42] X. Meng, Q. Yu, G. Liu, L. Shi, G. Zhao, H. Liu, P. Li, K. Chang, T. Kako, J. Ye, *Nano Energy* **2017**, *34*, 524.

Manuscript received: October 13, 2022

Accepted manuscript online: November 29, 2022

Version of record online: December 16, 2022